Solvatochromism of a Novel Betaine Dye Derived from Purine

Anna Masternak,[†] Grazyna Wenska,[†] Jan Milecki,[†] Bohdan Skalski,*,[†] and Stefan Franzen*,[‡]

Department of Chemistry, Adam Mickiewicz University, Poznan, Poland, and Department of Chemistry,
North Carolina State University, Raleigh, North Carolina 27695

A novel solvatochromic betaine dye has been synthesized from xanthosine and characterized spectroscopically by UV−vis in a broad range of solvents. The dye 9-(2′,3′,5′-tri-O-acetyl-β-D-ribofuranosyl)-2-(pyridinium-1-yl)-9H-purin-6-olate, **1a**, exhibits solvent-induced spectral band shifts that are $^2/_3$ as large as that of the betaine known as Reichardt's dye, which forms the basis of the $E_T(30)$ solvent polarity scale. Moreover, the dye **1a** is a ribonucleoside and hence has the potential application as a polarity probe for application in RNA oligonucleotides. The isomeric dye 6-(pyridinium-1)-yl-9H-purin-2-olate, **2a**, has also been synthesized and exhibits slightly smaller solvatochromic band shifts. The new betaine dyes have also been studied by comparing the experimental and calculated solvatochromic shifts based on the calculation of the UV/vis absorption spectra, using a combination of methods with density functional theory (DFT). The COSMO continuum dielectric method, an applied electric field term in the Hamiltonian, and time-dependent density functional theory (TD-DFT) methods were used to obtain absorption energies, ground-state dipole moments, and the difference dipole moment between the ground and excited states. The calculations predict a lower energy absorption band of charge-transfer character that is highly solvatochromic, and a higher energy absorption band that has $\pi-\pi^*$ character which is not solvatochromic, in agreement with the experimental data. For Reichardt's dye the difference dipole moment between the ground and excited state ($\Delta\mu = \mu_e - \mu_g$) was also calculated and compared to experiment: $\Delta\mu$(calcd) = −6 D and $\Delta\mu$(exptl) = −9 ± 1 D.[1] The ground-state dipole moment was found to be μ_g(calcd) = 18 D and μ_g(exptl) = 14.8 ± 1.2 D.[1]

Introduction

Solvatochromic[1] dyes have played an important role in the understanding of solvent polarity effects and are increasingly important as probes of complex biological systems.[2−4] The importance of such dyes is evident in part from the large number of solvent polarity scales that have been derived based on different dye molecules.[5] The most widely applied system has been that based on the betaine dye 2,6-diphenyl-4-(2,4,6-triphenylpyridinium-1-yl)phenolate (Reichardt's dye).[6,7] The E_T-(30) solvent polarity scale is based on the large shifts of the long-wavelength visible absorption band of this dye in a variety of solvents.[8] Such solvent polarity effects arise when there is a large ground-state dipole moment, μ_g, and a large difference between the dipole moments of the ground and excited states, $\Delta\mu = \mu_e - \mu_g$, where μ_e is the excited-state dipole moment. The ground-state dipole moment causes the reorientation of solvent molecules to produce a large reaction field, **G**.[9] The reaction field, in turn, results in a shift between the energies of the ground and excited state if their dipole moments differ. Thus, the shift in the transition wavenumber, Δ, is approximately proportional to $-\Delta\mu \cdot \mathbf{G}/hc$, where h is Planck's constant and c is the speed of light. Reichardt's betaine dye meets both of these criteria. Such betaine dyes are zwitterionic molecules and, therefore, have a substantial ground-state dipole moment, $\mu_g \approx$ 15 D. The relatively large charge-transfer character of the ground state provides the possibility of charge recombination in the excited state that leads to the observed dipole moment change

of $\Delta\mu \approx -$ 9 D for 2,6-diphenyl-4-(2,4,6-triphenylpyridinium-1-yl)phenolate determined both by solvatochromism and electrochromism.[10,11]

Reichardt's dye is one of a small number of molecules for which a comparison has been made of the solvatochromic and electrochromic effects. Electrochromism is the study of frequency shifts and line broadening that occurs in an externally applied electric field. Electrochromism provides information on the difference dipole moment, $\Delta\mu$, from the magnitude of the second-derivative line-shape change in an applied electric field. Thus, electrochromism provides a method to directly measure one of the quantities of interest in solvatochromism.[12]

It is interesting to consider betaine dyes that are analogues of Reichardt's dye and have similar solvatochromic properties, but can be used as probes of solvent polarity in biological systems and on surfaces. In this study, we discuss two such dyes based on the isomeric pyridinium-purinolate betaine structures shown in Scheme 1. These pyridinium-purinolate betaines are expected to have similar solvatochromic properties to Reichardt's dye. The solubility of **1a** and **2a** in polar solvents including water is very high, but they dissolve to a lesser degree in less polar organic solvents and they are insoluble in hydrocarbons. Compounds **1a** and **2a** are nucleosides and thus have potential application as probes of the solvent exposure of oligonucleotide structures in solution. Both Reichardt's dye and the pyridinium-purinolate betaines are strong hydrogen bond acceptors leading to substantially different behavior in hydrogen-bond donating (HBD) solvents.

In addition to the zwitterionic forms indicated in Scheme 1, compounds **1a,b** and **2,b** can be protonated, whereas **1b** and

* To whom correspondence should be addressed.
[†] Adam Mickiewicz University.
[‡] North Carolina State University.

SCHEME 1:   Molecular Structures of Betaine Dyes 1 and 2

1 a,b,c   **2 a,b,c**

a   R = 2',3',5'-tri-O-acetyl-β-D-ribofuranosyl   a   R = β-D-ribofuranosyl
b   R = H   b   R = H
c   R = CH₃   c   R = CH₃

2b can be additionally deprotonated to form the respective cationic and anionic forms, as indicated in Scheme 2.

In the present study we have used density functional theory methods to determine the ground-state dipole moment, μ_g, and difference dipole moment, $\Delta\mu = \mu_e - \mu_g$. The values obtained were compared with that of Reichardt's dye as well since experimental data are available for a comparison with the pyridinium-purinolate betaines. The calculation of these properties provides a method for predicting properties of solvatochromic molecules.

Experimental Methods

The spectroscopic grade (Merck) solvents methanol, ethanol, 2-propanol, 1-butanol, acetone, dimethyl sulfoxide, pyridine, dichloromethane, ethyl acetate, and trichloromethane and HPLC grade acetonitrile (Scharlau) were used as received. Water was doubly distilled and purified by using a Millipore Super Q system. The samples for spectroscopic studies were purified by HPLC (Waters) equipped with a Waters 991 Photodiode Array Absorption detector. The HPLC analyses were carried out on a reversed phase column HPLC XTerra RP₁₈ 7μm; 150 × 19 mm. UV/vis absorption spectra were recorded with a Cary 300 Bio (Varian) spectrophotometer. NMR spectra were measured with a Varian Unity 300 (300 MHz) spectrometer. ¹H and ¹³C chemical shifts (δ ppm) are referred to Si(CH₃)₄. Electrospray ionization mass spectra (ESI-MS) were recorded on a AMD Intectra Model 604.

Synthesis of the Betaine Dyes. 9-(2′,3′,5′-Tri-O-acetyl-β-D-ribofuranosyl)-2-(pyridinium-1-yl)-9H-purin-6-olate (**1a**) was obtained as described elsewhere.[13]

2-(Pyridinium-1-yl)-9H-purin-6-olate (**1b**). 9-(2′,3′,5′-Tri-O-acetyl-β-D-ribofuranosyl)-2-(pyridinium-1-yl)-9H-purin-6-olate (**1a**) (50 mg, 0.11 mmol) was dissolved in 0.1 M aqueous HCl (ca. 50 mL) and the solution left at room temperature for two weeks. After this time, HPLC analysis revealed complete conversion of **1a** to **1b**. Pure product was isolated from the neutralized reaction mixture by HPLC: mobile phase, 5% aqueous CH₃CN for 13 min followed by 80% aqueous CH₃CN for 2 min; flow rate, 3 mL/min.
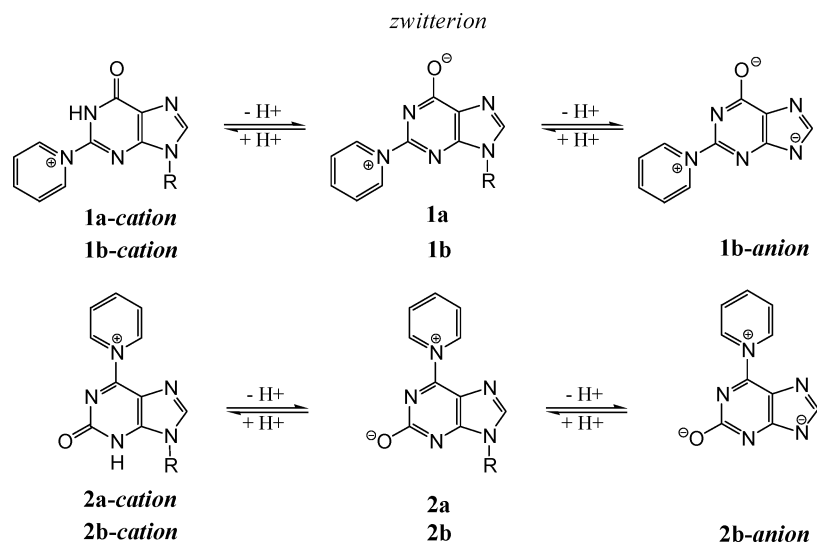
¹H NMR (D₂O) δ (ppm) 9.78 (d, J = 5.50 Hz, 2, α-H), 8.76 (t, J = 7.70 Hz, 1, γ-H), 8.19 (m, 3, β-H and 8-H); ¹³C NMR (D₂O) δ (ppm) 154.38 (C-6), 150.87 (C-γ), 150.22 (C-2), 144.89 (C-8), 143.54 (C-α), 139.07 (C-4), 130.11 (C-β), 126.84 (C-5); ESI-MS m/z 214.00 (M + H⁺), C₁₀H₈N₅O requires m/z 214.07.

9-(β-D-ribofuranosyl)-6-(pyridinium-1-yl)-9H-purin-2-olate (**2a**). Compound **2a** was obtained by treatment of N-[9-(2′,3′,5′-tri-O-acetyl-β-D-ribofuranosyl)-6-chloro-2-hydroxypurine (120 mg; 0.28 mmol) with dry pyridine (2 mL) at 60 °C for 5 h. Because of partial deprotection of the nucleoside, the crude mixture was treated overnight with 2.5% aqueous ammonia at room temperature. Pure deacetylated nucleoside **2a** was isolated in 16% yield from the concentrated reaction mixture by preparative HPLC: mobile phase, 27% aqueous CH₃CN; flow rate, 2 mL/min.

¹H NMR (D₂O) δ (ppm) 9.74 (d, 2, α-H), 8.80 (t, 1, γ-H), 8.28 (t, 2, β-H), 8.25 (s, 1, 8-H), 5.96 (d, 1, 1′-H), 4.80 (t, 1, 2′-H), 4.40 (m, J = 4.1 Hz, 3′-H), 4.23 (m, 1, 4′-H), 3.89–3.79 (m, 2, 5′,5″-H); ¹³C NMR (D₂O) δ (ppm) 165.76 (C-2), 157.92 (C-4), 149.41 (C-γ), 148.00 (C-6), 143.54 (C-8), 142.84 (C-α), 128.01 (C-β), 116.55 (C-5), 88.28 (C-1′), 85.80 (C-4′), 73.20 (C-2′), 70.63 (C-3′), 61.50 (C-5′); ESI-MS m/z 346.00 (M + H⁺), C₁₅H₁₆N₅O₅ requires m/z 346.11.

2-(Pyridinium-1-yl)-9H-purin-6-olate (**2b**). Compound **2b** was obtained with 90% yield by treatment of N-(2-aminopurin-6-yl)pyridinium chloride[14] (100 mg, 0.40 mmol) in aqueous solution (10 mL) with equimolar amounts of concentrated HCl and NaNO₂ (33%; w:w). The reaction mixture was then neutralized and concentrated under reduced pressure, and the crude product was precipitated by addition of acetone. The product was purified by HPLC: mobile phase, H₂O; flow rate, 3 mL/min.

¹H NMR (D₂O) δ (ppm) 9.66 (d, J = 5.50 Hz, 2, α-H), 8.68 (t, 1, γ-H), 8.16 (t, J = 7.69 Hz, 2, β-H), 8.05 (s, 1, 8-H); ¹³C

SCHEME 2:   Acid−Base Equilibria of Betaine Dyes 1a,b and 2a,b

zwitterion

1a-*cation*   **1a**   **1b-*anion***
1b-*cation*   **1b**

2a-*cation*   **2a**   **2b-*anion***
2b-*cation*   **2b**

Solvatochromism of a Novel Betaine Dye

J. Phys. Chem. A, Vol. 109, No. 5, 2005 **761**

NMR (D$_2$O) δ (ppm) 166.03 (C-2), 159.23 (C-4), 150.48 (C-γ),148.41 (C-6), 146.70 (C-8), 143.67 (C-α), 128.91 (C-β), 117.58 (C-5); ESI-MS *m/z* 214.00 (M + H$^+$), C$_{10}$H$_8$N$_5$O requires *m/z* 214.07.

Computational Methods

A combination of Density Functional Theory (DFT) and Time-Dependent Density Functional Theory (TD-DFT) methods were employed to study spectroscopic properties of the xanthine pyridinium betaines. The optimized ground-state geometries and potential energy surfaces of **1b,c**, **2b,c**, and related molecules were obtained by using the GGA functional[15] as implemented in DMol3 (Molecular Simulations Inc.).[16,17] Calculations were carried out on the Blade Cluster at the North Carolina State University High Performance Computing Center. Geometry optimizations were carried out without constraints until the energy difference was less than 10^{-6} au on subsequent iterations (Supporting Information). A numerically tabulated basis set of double-ζ plus polarization (DNP) quality was employed as described in the Supporting Information.

The models used include the 9-methyl-2-(pyridinium-1-yl)-9*H*-purin-6-olate, **1c**, and 9-methyl-6-(pyridinium-1-yl)-9*H*-purin-2-olate, **2c**, for the spectroscopic, solvatochromic, and electrochromic properties as well as the pyridinium-purinolates **1b** and **2b**, with a hydrogen atom at the N9 position, for the pH dependence as shown in Scheme 1. Test calculations were carried out with the ribose instead of the methyl group in the 9-position of the purine ring. As expected the substitution of methyl for ribose has a negligible effect on the spectroscopic and electrochromic properties. The reason for this is that the molecular orbitals involved in the observed transitions are all of $\pi-\pi$* character and when they involve charge transfer there is only a minor contribution from hyperconjugation in the N9 position of the ring. The electrochromism calculations were carried out only for the **1c** and the structural isomer **2c** because of the economy of calculation (replacing ribose with methyl) with negligible effect on the results. The number of basis functions for a calculation of **1c** is 283 while for **1a** it is 425. The pH dependence of the absorptive transitions (e.g., for the series **1b**, **1b**-cation, and **1b**-anion) was calculated with both DFT and TD-DFT, but no solvatochromism or electrochromism was carried out for molecules **1b** or **2b**.

For the calculation of difference dipole moments, the transition energies were calculated with DFT methods (DMol3) at two values of the electric field oriented along the three Cartesian coordinates. The electric field term is included in the Hamiltonian and results in a shift in the energy of both occupied and unoccupied levels that results in a shift of transition energies. Representing the energy of a particular transition at an applied electric field of $F_{\gamma\pm}$ ($\gamma = x$, y, or z) as $E(F_{\gamma\pm})$, the average of the difference in the transition energy was calculated based on the results of DFT calculations according to eq 1. The applied

$$\Delta E = \frac{E(F_{x+}) - E(F_{x-}) + E(F_{y+}) - E(F_{y-}) + E(F_{z+}) - E(F_{z-})}{3}$$

$$(1)$$

field used in the calculations was ± 0.001 au (1 au = 5.29 $\times$ 10^9 V/cm). The conversion to difference dipole moment uses the factor $\Delta\mu = \Delta E$ (in cm^{-1})/169.7 D. This approach was used rather than attempting to define the direction of the difference dipole moment and then to align the molecule in the applied electric field. The average of the field application in the three

Cartesian directions as presented in eq 1 is assumed to give the same effect as aligning the molecule in the applied field. In all cases (including Reichardt's dye) the orientation of the ground-state dipole moment is approximately aligned from the pyridinium ring nitrogen atom (+) to the oxygen atom (−). The difference dipole moment has the opposite polarity in all cases, leading to a net decrease in the dipole moment in the excited state.

Solvation is an important factor in the stabilization of charge-transfer states. Solvation energies were calculated by using a dielectric continuum model (COSMO)[18,19] implemented in DMol3. The transition energies were calculated in DMol3 for various values of the continuum relative permittivity, ϵ_r, ranging from $\epsilon_r = 1$ to 80. The ground-state dipole moment, μ_g, was obtained at each value of the relative permittivity and the difference dipole moment was calculated as indicated above in eq 1 for each value of ϵ_r as well.

Time-dependent density function theory (TD-DFT) calculations were carried out with the program ORCA,[20,21] using the Ahlrich basis set.[22] The TD-DFT calculations were used to determine which states contribute to the observed UV/vis absorption spectrum. The TD-DFT calculations were used to determine which transitions were important for the observed spectroscopic transitions. Fortunately, there was usually a dominant transition in the cases studied here (i.e. a transition that comprised 80% or more of the observed transition intensity). The transition energies obtained by TD-DFT with ORCA are in much closer agreement with experiment than those obtained by DFT methods using DMol3. In summary, the transition energies were obtained by TD-DFT, but dipole moment, μ_g, and difference dipole moment, $\Delta\mu$, were obtained by using DMol3 as a function of relative permittivity, ϵ_r.

Results

The betaines **1a** and **2a** shown in Scheme 1 were obtained by a hydrolysis of the purine dipyridinium salts in basic aqueous medium[13] followed by deribosylation (**1b**), by deamination of aminopurine pyridinium chloride (**2b**), or by substitution of a halogen in the appropriate chlorohydroxypurine riboside by the pyridine residue (see Experimental Section). The UV/vis absorption spectra of all new compounds were measured in several organic solvents as well as in water. The spectrum of each betaine in any of the solvents used consists of two absorption bands located at $\tilde{\nu}_{max} = 42\,016-40\,816$ cm^{-1} (λ_{max} = 238−245 nm) and $\tilde{\nu}_{max} = 29\,850-24\,630$ cm^{-1} (λ_{max} = 335−406 nm) in the case of **1a** and **1b**, and $\tilde{\nu}_{max} = 37\,313-36\,630$ cm^{-1} (λ_{max} = 268−273 nm) and $\tilde{\nu}_{max} = 26\,595-22\,222$ cm^{-1} (λ_{max} = 376−450 nm) for **2a** and **2b**. The intensity of the higher energy band is approximately twice as large as that of the lower energy band. Only the solvatochromism of the long-wavelength absorption band was measured because the position of the higher energy band does not change significantly with solvent polarity. The normalized long-wavelength UV/vis absorption bands of **1a** and **2a** in five selected solvents of different polarity are presented in Figure 1, parts a and b. The absorption maxima measured in 12 solvents as well as the solvent's Onsager polarity function [f(ϵ_r) − f(n^2)] are presented in Table 1. Inspection of the data presented shows that the betaines **1a** and **1b** absorb at higher energy (shorter wavelength) than their respective isomers **1b** and **2b**, but they all exhibit similar negative solvatochromism, i.e., a hypsochromic band shift with increasing solvent polarity.

The dependence of the absorption maximum ($\tilde{\nu}_{max}$ [cm^{-1}]) of **1a,b** as well as **2a,b** on the Onsager solvent polarity function can be fitted to a linear function. However, the correlation for
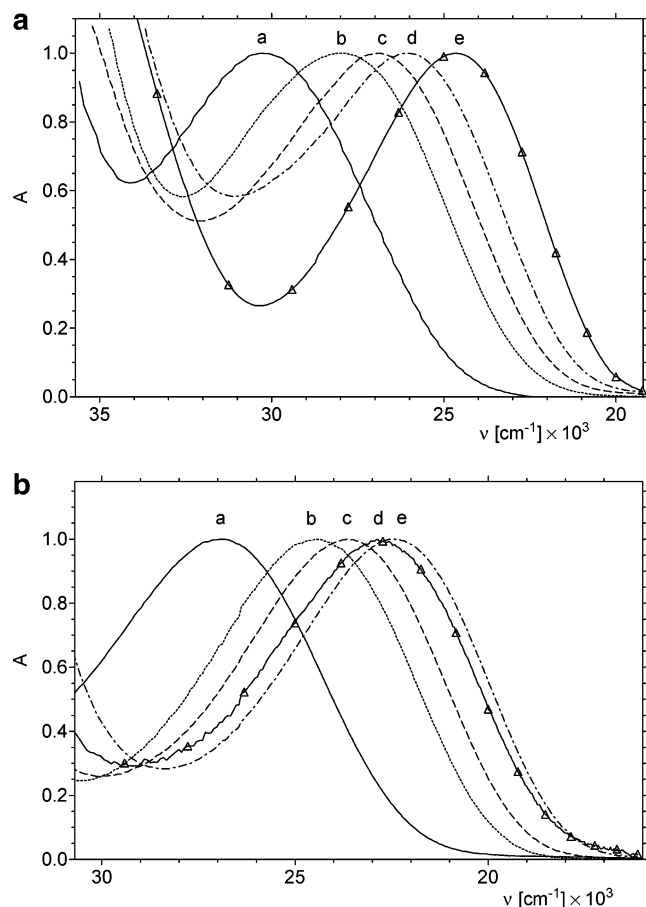
Figure 1. (a) Normalized long-wavelength UV/vis absorption band of **1a** in five selected solvents: a, water; b, ethanol; c, 1-butanol; d, dimethyl sulfoxide; and e, trichloromethane. (b) Normalized long-wavelength UV/vis absorption band of **2a** in five selected solvents: a, water; b, ethanol; c, 1-butanol; d, acetonitrile; and e, dimethyl sulfoxide.

**TABLE 1: Solvent Effect on the Position of the Long-Wavelength UV/Vis Absorption Maximum of 1a,b and 2a,b**[a]

solvent	rel permittivity	$f(\epsilon_r) - f(n^2)$[b]	$\tilde{\nu}^A_{max}$ [cm^{-1}]			
			1a	2a	1b	2b
H$_2$O	80.16	0.319	29851	26950	29940	26600
CH$_3$OH	32.66	0.309	28571	24880	28090	24750
C$_2$H$_5$OH	24.55	0.289	28090	24510	27933	24690
i-C$_3$H$_7$OH	19.92	0.276	26738	23470	27100	23750
C$_4$H$_9$OH	17.51	0.268	26882	23640	27248	23810
(CH$_3$)$_2$SO	46.45	0.263	25907	22470	25707	22830
CH$_3$CN	35.94	0.305	25907	22880	26247	22780
(CH$_3$)$_2$CO	20.56	0.284	25974	22780	25575	
C$_5$H$_5$N	12.91	0.214	24510		24272	
CH$_2$Cl$_2$	8.93	0.217	24630		25316	22220
CH$_3$COOC$_2$H$_5$	6.02	0.199	24272			
CHCl$_3$	4.806	0.149	24630		24938	22220

[a] The relative permittivity[28] of each solvent is listed in column 2. [b] $f(\epsilon_r) - f(n^2) = (\epsilon_r - 1)/(2\epsilon_r + 1) - (n^2 - 1)/(2n^2 + 1)$; ϵ_r = relative permittivity, n = refraction index.

protic (=HBD) solvents (Figure 2a) differs from that for aprotic solvents (Figure 2b). The equations describing the correlation of $\tilde{\nu}_{max}$ [cm^{-1}] of **1a,b** and **2a,b** in several HBD and non-HBD solvents are presented in the Supporting Information. The slopes obtained from linear regression analysis of the plots $\tilde{\nu}_{max}$ vs [$f(\epsilon_r) - f(n^2)$] in HBD solvents are significantly (4−10 times) higher than that in non-HBD solvents as is evident also from an inspection of Figure 2.

The UV/vis absorption spectra of **1a,b** and **2a,b** were also measured in aqueous solution as a function of pH from pH 1 to
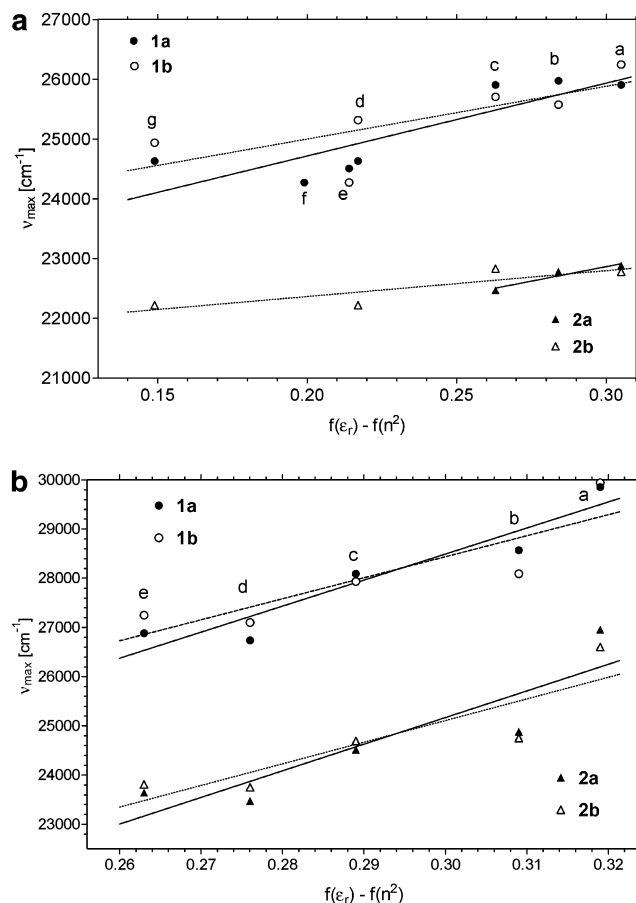
Figure 2. (a) Plot of the wavenumber of the longest wavelength UV/vis absorption band, $\tilde{\nu}_{max}$, against the solvent's Onsager orientation polarization function, $f(\epsilon_r) - f(n^2)$, for seven non-HBD solvents: a, acetonitrile; b, acetone; c, dimethyl sulfoxide; d, methylene chloride; e, pyridine; f, ethyl acetate; and g, trichloromethane. (b) Plot of the wavenumber of the longest wavelength UV/vis absorption band, $\tilde{\nu}_{max}$, against the solvent's Onsager orientation polarization function, $f(\epsilon_r) - f(n^2)$, for five HBD solvents: a, water; b, methanol; c, ethanol; d, 2-propanol; and e, butanol.

13. In basic media (pH >8), the changes in the spectra were observed only for the betaines **1b** and **2b**, which possess a N(9)−H instead of ribose in the N(9) position in **1a** and **2a**. The selected UV/vis spectra for **1b** are presented in Figure 3, parts a and b. In acidic media the lowest energy band of **1b**, like that of the other betaine dyes, shifts to the blue without significant change in its intensity. The absorbance at shorter wavelengths increases and a distinct peak at $\tilde{\nu} = 38\,000$ cm^{-1} ($\lambda = 263$) nm is observed in the case of **1b**-cation (Figure 3a), while in the case of **1b**-anion the intensity of the short wavelength peak at $\tilde{\nu} \approx 37\,037$ cm^{-1} ($\lambda \approx 270$ nm) decreases (data not shown). The changes observed in the UV/vis absorption spectra of the betaines in acidic solution are due to protonation at N(1) in the purine ring (Scheme 2). The set of UV/vis spectra recorded for each betaine dye as a function of pH in acidic medium shows one isosbestic point for each dye, indicating that only two species are involved in the cation D zwitterion equilibrium. The absorption spectral characteristics of the cationic species derived from the betaines and the ground-state pK_a values determined by spectrophotometric titration are presented in Table 2 and those for **1b** in the inset in Figure 3a.

In basic solutions (pH >8), the longest wavelength band maximum of **1b** and **2b** shifts gradually to longer wavelength as the pH increases. Under these conditions the zwitterionic molecules undergo deprotonation to give anions (Scheme 2).

Solvatochromism of a Novel Betaine Dye

J. Phys. Chem. A, Vol. 109, No. 5, 2005 **763**

TABLE 2: pH Effect on the Long-Wavelength UV/Vis Absorption Maximum of 1a,b and 2a,b and pK_a Values for Zwitterion−Cation and Zwitterion−Anion Equilibrium

| | $\tilde{\nu}^A_{max}$ [cm^{-1}] (ϵ [M^{-1} cm^{-1}]) | | | pK_a | |
compd	cation	zwitterion	anion	zwitterion−cation	zwitterions−anion
1a	33 000 (5 280)	29 851 (4 000)		2.3	
1b	32 680 (3 740)	29 940 (3 430)	27 030 (3 730)	3.01	10.64
2a	30 300 (3 960)	26 950 (3 320)		4.05	
2b	29 410 (2 780)	26 600 (3 200)	24 690 (2 950)	4.60	9.83

The set of UV/vis spectra recorded for **1b** in basic solutions is presented in Figure 3b. The spectral characteristics of anions and the pK_a values characterizing the ground-state zwitterions− anion equilibrium determined from the absorption spectra are included in Table 2.

The transition energy for **1c** was calculated as a function of the continuum relative permittivity, ϵ_r, calculated by using DFT methods including the COSMO continuum dielectric model.[18,19] The details are reported in the Supporting Information. The lowest four transitions have transition energies that depend strongly on ϵ_r. The TD-DFT calculation on **1c** revealed that there is one intense electronic transition at $\tilde{\nu}_{max} = 25\,735$ cm^{-1} ($\lambda_{max} = 388$ nm) that is comprised 87% of the transition from MO $54 \rightarrow 60$, which is a transition with a large charge-transfer character. In the transition $54 \rightarrow 60$ the electron density is displaced from the purine ring to the pyridinium ring. The next

two higher transitions show weak or no dependence on the relative permittivity of the solvent. The TD-DFT calculations reveal that a band should be observed at $\tilde{\nu}_{max} = 37\,267$ cm^{-1} ($\lambda_{max} = 267$ nm) that is comprised 82% of the transition from MO $59 \rightarrow 62$. This transition is predominately a $\pi - \pi^*$ transition as can be seen in Figure 4. In summary, the combination of
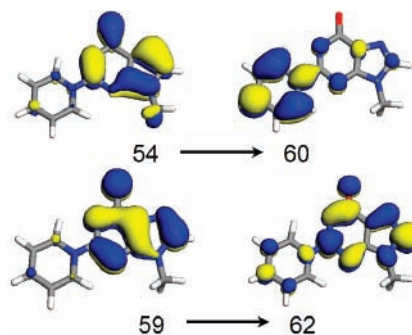
Figure 4. The molecular orbitals for the two electronic transitions of **1c** obtained from the DFT calculations. The transition from MO $54 \rightarrow 60$ corresponds to the observed solvatochromic band. The transition from MO $59 \rightarrow 62$ corresponds to the higher energy band that shows little solvent dependence.
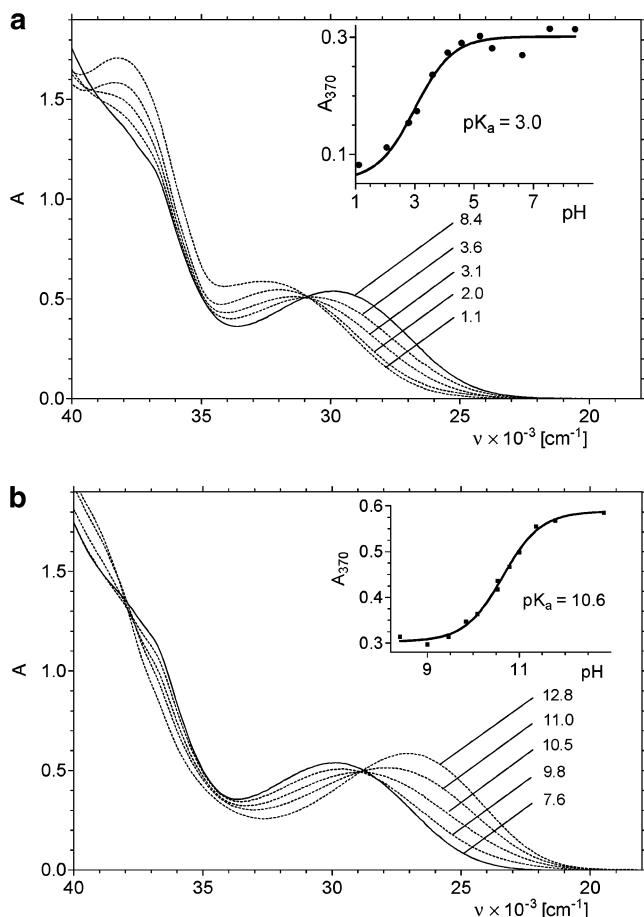
DFT (DMol3) and TD-DFT (ORCA) calculations predicts two intense absorption bands for **1c**. The lower energy band is predicted to occur at $\tilde{\nu}_{max} = 25\,735$ cm^{-1} ($\lambda_{max} = 388$ nm) and should be highly solvatochromic. The spectra in Figure 1a show that a band is indeed observed in the range $\tilde{\nu}_{max} = 29\,411 - 24\,390$ cm^{-1} ($\lambda_{max} = 340-410$ nm) (depending on the solvent) that is highly solvatochromic. The higher energy band at 37 267 cm^{-1} ($\lambda_{max} = 267$ nm) that is predicted to be unaffected by solvent can be compared to the observed **1a** band at 42 017 cm^{-1} ($\lambda_{max} = 328$ nm) in water that is indeed not shifted by more than $\Delta\tilde{\nu} = 1200$ cm^{-1} to the red in the solvents used in this study (in CH$_2$Cl$_2$: 40 816 cm^{-1}; data not shown). The isosurfaces for the molecular orbitals (MOs) for the remaining transitions are presented in the Supporting Information.

The electronic transitions in **2c** show larger calculated changes in intensity with a increase in the relative permittivity of the solvent than **1c**, for which the intensities were relatively constant. The transitions from MO $51 \rightarrow 60$, $52 \rightarrow 60$, and $53 \rightarrow 60$ are all close in energy and appear to change their character as the continuum relative permittivity is altered in the COSMO calculation. We have not attempted to perform a detailed analysis of this effect because these transitions do not correspond to the solvatochromic transition.

The TD-DFT calculation for **2c** yields three intense bands. The band at $\tilde{\nu}_{max} = 22\,252$ cm^{-1} ($\lambda_{max} = 449$ nm) is comprised of 95% of the transition from MO $56 \rightarrow 60$. This transition is highly dependent on the solvent's relative permittivity based on the COSMO calculation and is clearly the analogue of the transition at $\tilde{\nu}_{max} = 25\,735$ cm^{-1} ($\lambda_{max} = 388$ nm) in **1c**. The solvatochromic band of **2a** is indeed shifted to longer wavelength as predicted by this calculation and is observed in the

Figure 3. (a) The pH dependence of the absorption spectra of **1b** and **1b**-cation; aqueous buffer solutions $1.1 < 1$ pH < 8.4 at room temperature. Inset: Spectrophotometric titration curve plotted as absorption intensity at 370 nm vs pH. (b) The pH dependence of the absorption spectra of **1b** and **1b**-anion; aqueous buffer solutions, $12.84 > pH > 7.55$ at room temperature. Inset: Spectrophotometric titration curve plotted as absorption intensity at 370 nm vs pH.

TABLE 3: The Difference Dipole Moments, $\Delta\mu$, in Debye Calculated by Using the Band Shifts of Electronic Transition in an Applied Electric Field, and Calculated Ground-State Dipole Moments, μ_g, for the Dye Molecules 1c, 2c, and Betaine Dye 30 (Reichardt's dye)

	$\epsilon_r = 1$	$\epsilon_r = 10$	$\epsilon_r = 20$
1c transition			
$\Delta\mu$ for $54 \rightarrow 60$	−4.4	−8.0	−8.2
$\Delta\mu$ for $59 \rightarrow 62$	−0.89	−0.40	−0.32
ground-state μ_g	12.5	17.5	18.1
2c transition			
$\Delta\mu$ for $56 \rightarrow 60$	−3.0	−6.4	−6.7
$\Delta\mu$ for $59 \rightarrow 62$	−1.2	−1.6	−1.8
$\Delta\mu$ for $52 \rightarrow 60$	−2.3	−1.4	−5.4
ground-state μ_g	10.5	14.9	15.4
betaine dye 30 transition			
$\Delta\mu$ for $145 \rightarrow 146$	−1.9	−5.6	−6.1
ground-state μ_g	10.5	18.3	19.2

TABLE 4: Calculated Absorption Maxima and Orbital Character for the Protonation States of 1b[a]

compd	λ_{max} (nm)	root	character
1b	413.2	9	74% $50 \rightarrow 56$
			21% $52 \rightarrow 57$
1b-cation	314.6	6	80% $51 \rightarrow 56$
1b-cation	248.6	13	67% $55 \rightarrow 58$
1b-anion	418.5	12	53% $50 \rightarrow 56$
			36% $52 \rightarrow 57$

[a] Only the first 20 roots were calculated with the TD-DFT program ORCA. The orbital character is reported for each transition.

range from $\tilde\nu_{max} = 27\,027$ to $22\,222$ cm^{-1} ($\lambda_{max} = 370-450$ nm). A band is also predicted from the TD-DFT calculation at $\tilde\nu_{max} = 29\,181$ cm^{-1} ($\lambda_{max} = 343$ nm), which is calculated to be 82% MO $59 \rightarrow 62$, and in addition there is a transition calculated to occur at $\tilde\nu_{max} = 34\,784$ cm^{-1} ($\lambda_{max} = 287$ nm), which is composed 81% of the transition from MO $52 \rightarrow 60$. The COSMO calculation suggests that the UV/vis band at $\tilde\nu_{max} = 29\,181$ cm^{-1} ($\lambda_{max} = 343$ nm) should show about one-half of the solvatochromic shift observed for the band at $\tilde\nu_{max} = 22\,252$ cm^{-1} ($\lambda_{max} = 449$ nm). The UV/vis band calculated at $\tilde\nu_{max} = 34\,784$ cm^{-1} ($\lambda_{max} = 287$ nm) should show essentially no solvatochromic shift.

The calculated ground-state dipole moments, μ_g, and difference dipole moments, $\Delta\mu$, as a function of the relative permittivity are presented in Table 3 for both **1c** and **2c**. The difference dipole moments, $\Delta\mu$, were calculated from the electric field dependence as indicated in the Methods section. The difference dipole moments scale approximately with the observed solvatochromic shifts as expected from the reaction field. There is a substantial difference between the vacuum calculation ($\epsilon_r = 1$) and the calculations at higher relative permittivities. For example, for **1c** the difference dipole moment of the HOMO $\rightarrow$ LUMO transition is $\Delta\mu = -12.5$ D for the vacuum calculation ($\epsilon_r = 1$) and -18.1 D for a solvent relative permittivity of $\epsilon_r = 10$. Since the observed difference dipole moment is obtained from solvatochromic measurements (i.e. not in a vacuum), the combination of electric fields and the COSMO dielectric continuum model was used to obtain a more realistic model.

As a check on the values we have also performed the same calculations on the betaine 30 dye molecule (Reichardt's dye) used for the $E_T(30)$ solvent polarity scale. Both the ground-state dipole moment and difference dipole moment for the dye betaine 30 have been determined to be $\mu_g \approx 15$ D and $\Delta\mu \approx -9$ D by using solvatochromism (Mataga equation) and $\mu_g \approx 15$ D and $\Delta\mu \approx -9$ D by electroabsorption spectroscopy.[1] The values obtained by calculation in a medium of relative permittivity of $\epsilon_r = 10$, shown in Table 4, are $\mu_g \approx 18$ D and $\Delta\mu \approx -6$ D, using the same analysis presented above for the pyridinium-purinolate betaines.

The pH dependence of the pyridinium-purinolate betaine bases (without the ribose sugar) was also investigated both experimentally and with DFT methods. The electronic transitions of the molecule **1b** were calculated and compared to models for the protonated (**1b**-cation) and deprotonated (**1b**-anion) forms that represent the structures at pH <5.0 and >9.0, respectively (Scheme 2). The output transitions and isosurfaces for the relevant molecular orbitals are presented in the Supporting

Information. The character of the transitions for **1b** is completely analogous to those of the 9-methyl derivative (**1c** shown above). Inspection of the absorptive transitions in Figure 3 reveals that the major change occurs between the protonated (low pH) form and the neutral (pH 7.0) form. This calculated trend using the TD-DFT method presented in Table 4 is in agreement with this observation. The low pH form (**1b**-cation) has two calculated transitions at $\tilde\nu_{max} = 40\,160$ and $31\,746$ cm^{-1} ($\lambda_{max} = 249$ and 315 nm). The higher energy transition has no charge-transfer character and is not predicted to be solvatochromic, while the calculated band at $\tilde\nu_{max} = 31\,746$ cm^{-1} ($\lambda_{max} = 315$ nm) is predicted to have charge-transfer character. The observed UV/vis bands in **1b**-cation are at $\tilde\nu_{max} = 32\,680$ cm^{-1} ($\lambda_{max} = 306$ nm) and $\tilde\nu_{max} = 38\,000$ cm^{-1} ($\lambda_{max} = 263$ nm). In the neutral pH form **1b** the higher energy transition is not found within the first 20 roots and must be higher in energy than $\tilde\nu = 38\,910$ cm^{-1} ($\lambda = 257$ nm) according to the calculation (see Supporting Information). However, the lower energy band is calculated to shift from $\tilde\nu_{max} = 31\,750$ cm^{-1} ($\lambda_{max} = 315$ nm) (**1b**-cation) to $\tilde\nu_{max} = 24\,213$ cm^{-1} ($\lambda_{max} = 413$ nm) (**1b**). The observed shift is from $\tilde\nu_{max} = 32\,680$ cm^{-1} ($\lambda_{max} = 306$ nm) in **1b**-cation to $\tilde\nu_{max} = 29\,940$ cm^{-1} ($\lambda_{max} = 334$ nm) in **1b**, which is significantly smaller. The smaller shift arises from the fact that the TD-DFT calculation was carried out for a molecule in a vacuum and we did not perform the same combination of COSMO continuum dielectric and TD-DFT calculations for the protonation states of **1b** as were performed for the 9-methyl derivative, **1c**. The high pH form (**1b**-anion) is calculated to have $\tilde\nu_{max}$ at $23\,923$ cm^{-1} (λ_{max} at 418 nm). Thus, the shift from neutral (**1b**) to anionic (**1b**-anion) form is only calculated to be $\Delta\tilde\nu = 290$ cm^{-1} ($\Delta\lambda = 5$ nm = 418−413 nm). While this is substantially smaller than the observed shift of $\Delta\tilde\nu = 2910$ cm^{-1} (Table 2), the trends are reproduced in the calculation. Similar results were obtained for the calculated and observed spectra of **2b** (see Supporting Information). The lack of quantitative agreement with experiment can be attributed to the fact that these calculations were carried out in a vacuum ($\epsilon_r = 1$) and solvent effects (which probably also include hydrogen bonding) are certainly important determinants of the observed transition energy. Solvation effects that include specific solvent interactions would involve computations beyond the scope of the present study.

Discussion

The betaine dye **1a** is a simple solvatochromic probe molecule that has many unique features that make it comparable to the well-known betaine dye 30 or Reichardt's dye used to calibrate the $E_T(30)$ solvent polarity scale. It has a large ground-state dipole moment that is as large as that of betaine 30. Moreover, its difference dipole moment is estimated from both experiment and theory to be even larger than that of betaine dye 30. **1a** is quite water soluble and is also soluble in a broad range of polar and nonpolar solvents.

Solvatochromism of a Novel Betaine Dye

J. Phys. Chem. A, Vol. 109, No. 5, 2005 **765**

TABLE 5: Comparison of Calculated and Experimental Values for the Product $\mu_g\Delta\mu$ Related to the Magnitude of the Observed Solvatochromic Shift[a]

compd	$\mu_g\Delta\mu$ [D^2] (exptl)	μ_g [D] (calcd)	$\Delta\mu$ [D] (calcd)	$\mu_g\Delta\mu$ [D^2] (calcd)
1a[b]	151.4	17.4	−8.0	139.2
1b	109.7			
2a[b]	121.3	14.9	−6.4	95.4
2b	53.9			

[a] The calculated values compared in the table were obtained for a continuum relative permittivity of $\epsilon_r = 10$. [b] The calculated values were obtained for the methyl derivative. The experimental values were obtained for the riboside.

The origin of the solvatochromism is a combination of a large ground-state dipole moment, μ_g, and a large difference dipole moment, $\Delta\mu$. The large ground-state dipole moment creates a reaction field that is related to the solvent's relative permittivity according to the Onsager reaction field. We have calculated the difference dipole moment using an electric field term in the DFT Hamiltonian and compared the magnitude of the difference dipole moments. The calculated difference dipole moment for the observed transition of betaine 30 (Reichardt's dye) is presented in Table 3. At a relative permittivity of $\epsilon_r = 10$ we find a reasonable agreement with experimental electroabsorption studies of this molecule (Table 5). The calculated μ_g and $\Delta\mu$ are ∼18 D and ∼ −6 D, respectively, compared to experimental values of ∼15 D and ∼ −9 D.[10,11] Because of these properties betaine dye 30 has been studied as a model compound for excited-state dynamics of intermolecular charge transfer.[25−27] Table 3 also shows that the calculated values of μ_g and $\Delta\mu$ for **1c** are comparable to those of betaine dye 30, but smaller values are calculated for the structural isomer **2c** (see Scheme 1).

The calculated and experimental values for μ_g and $\Delta\mu$ can also be compared for **1c** and **2c** by using the solvatochromism data. From the slopes of the plots determined in non-HBD solvents a value of the product $\mu_g\Delta\mu$ was calculated by using the McRae equation:[23] $\mu_g\Delta\mu = $ slope $\times hca^3/2$, where $h = 6.63 \times 10^{-27}$ erg·s and $c = 3 \times 10^{10}$ cm/s. The values of $\mu_g\Delta\mu$ calculated from the experimental data assuming a cavity radius for the betaine dyes of $a = 5 \times 10^{-8}$ cm are presented in Table 5. The radius of 5 Å corresponds approximately to the radius of **1a** (or **2a**) and the first solvent shell. Thus, we see that the trends in the data are consistent with the DFT calculations of the spectra.

The magnitude of the solvent dependence is correlated with the charge-transfer character of the electronic transition. In **1c**, the HOMO → NLUMO transition (59 → 61) shows a large dependence on the solvent dielectric (calculated using the COSMO continuum dielectric) and a large calculated difference dipole moment using an applied electric field in the Hamiltonian. These properties can be explained by the MOs for states 54 and 60 shown in Figure 4. The orbital character of MO 59 is predominantly a purine ring π-type, while the character of MO 61 is largely a pyridinium π orbital. It is expected that such a transition will show large changes in geometry associated with the transition between the ground and excited states leading to a relatively small fluorescence yield. The fluorescence yield of **1a** is indeed very small ($\varphi_F < 10^{-4}$). Representative fluorescence spectra are presented in the Supporting Information. On the other hand, transitions that have small dipole moments and small band shifts, associated with the change in dye continuum relative permittivity, are also expected to exhibit a smaller change in the orbital character upon electronic transition. An example of this behavior can be seen for the transition from 59 → 62 in

1c, which is a $\pi-\pi^*$ transition centered on the purine ring. The results here show that the mechanism and behavior of **1a** (and the model compound **1c**) is completely analogous to that of Reichardt's dye. The charge-transfer character of Reichardt's dye that has long been discussed in the literature is consistent with the DFT calculations (see Supporting Information for representations of the isosurfaces of the MOs).

To compare the magnitudes of the solvent-induced band shifts of pyridinium-purinolate betaines and Reichardt's dye, the $\tilde{\nu}_{max}$ values measured in all solvents used in this work (Table 1) were plotted against the $E_T(30)$ parameter. The values of $\tilde{\nu}_{max}$ (cm^{-1}) for Reichardt's dye were obtained by transformation of the E_T-(30) values, which correspond to the position of the absorption band maximum (in kcal × mol^{-1}) in a particular solvent.[24] The slopes of the linear plots (see Supporting Information) obtained for **1a** ($r^2 = 0.96$) and **2a** ($r^2 = 0.95$) amount to 67% (**1a**) and 62% (**2a**) of the value obtained by linear regression analysis of the Reichardt's betaine plot, indicating that purinyl-pyridinium betaines are slightly less solvatochromic compounds than Reichardt's dye.

Conclusion

The present study documents a new solvatochromic dye called pyridinium-purinolate betaine. The properties of this betaine dye are remarkably similar to those of the much larger molecule known as Reichardt's dye used to calibrate the $E_T(30)$ solvent polarity scale. The fact that the dye is a nucleoside presents a range of possible new applications for the study of solvatochromism in biological systems. **1a** is a probe that can be used in DNA and RNA to obtain information on solvent exposure and, therefore, on changes in the structure of oligonucleotides. This is of particular interest in RNA where the dye molecule can be incorporated into oligonucleotides as a probe of RNA−RNA and RNA−protein interactions.

Supporting Information Available: Description of the basis set used in the DMol3 calculation, tabulation of output transition energies using both DFT (Dmol3) and TD-DFT (ORCA), representation of isosurfaces for relevant molecular orbitals, analysis data of difference dipole moments for **1c**, **2c**, and Reichardt's dye, comparison calculations using molecule **1a**, and fluorescence spectra for **1a**. This material is available free of charge via the Internet at http://pubs.acs.org.

References and Notes

(1) Liptay, W.; Dumbacher. B.; Weisenberger. H. *Z. Naturforsch. A: Phys. Sci.* **1968**, *A23*, 1601.

(2) Laage, D.; Thompson, W. H.; Blanchard-Desce, M.; Hynes, J. T. *J. Phys. Chem. A* **2003**, *107*, 6032.

(3) Fayed, T. A. *Colloids Surf. A* **2004**, *236*, 171.

(4) Yang, X.; Liu, W. H.; Jin, W. J.; Shen, G. L.; Yu, R. Q. *Spectrochim. Acta, Part A* **1999**, *55*, 2719.

(5) Katritzky, A. R.; Fara, D. C.; Yang, H.; Tamm, K. T.; Karelson, M. *Chem. Rev.* **2004**, *104*, 175.

(6) Reichardt, C. *Chem. Rev.* **1994**, *94*, 2319.

(7) Suppan, P. *J. Photochem. Photobiol., A* **1990**, *50*, 293.

(8) Dimroth, K.; Reichardt, C.; Siepmann, T.; Bohlmann, F. *Liebigs Ann. Chem.* **1963**, *661*, 1.

(9) Böttcher C. J. F. *Theory of Electric Polarization*, 2nd ed.; Elsevier: Amsterdam, The Netherlands, 1973; Vol. 1.

(10) Schweig, A.; Reichardt, C. *Z. Naturforsch. A: Phys. Sci.* **1966**, *21*, 1373.

766 *J. Phys. Chem. A, Vol. 109, No. 5, 2005*

Masternak et al.

(11) Liptay, W.; Schlosser. H.; Dumbacher. B.; Hünig, S. *Z. Naturforsch. A: Phys. Sci.* **1968**, *A 23*, 1613.

(12) (a) Liptay, W. *Angew. Chem.* **1969**, *81*, 195. (b) Liptay, W. *Angew. Chem., Int. Ed. Engl.* **1969**, *8*, 177.

(13) Skalski, B.; Wenska, G.; Gdaniec, Z.; Adamiak, R. W. *Tetrahedron* **1993**, *49*, 5859.

(14) Skalski, B.; Paszyc, S.; Adamiak, R. P.; Steer, R. E.; Verrall, P. *Can. J. Chem.* **1990**, *68*, 2164.

(15) Perdew, J. P.; Chevary, J. A.; Vosko, S. H.; Jackson, K. A.; Pederson, M. R.; Singh, D. J.; Fiolhais, C. *Phys. Rev. B: Condens. Matter* **1992**, *46*, 6671.

(16) Delley, B. *J. Chem. Phys.* **2000**, *113*, 7756.

(17) Delley, B. *J. Chem. Phys.* **1990**, *92*, 508.

(18) Neese, F. *J. Chem. Phys.* **2003**, *119*, 9428.

(19) Neese, F. *Curr. Opin. Cell Biol.* **2003**, *7*, 125.

(20) Schaefer, A.; Horn, H.; Ahlrichs, R. *J. Chem. Phys.* **1992**, *97*, 2571.

(21) Andzelm, J.; Kolmel, C.; Klamt, A. *J. Chem. Phys.* **1995**, *103*, 9312.

(22) Klamt, A.; Schuurmann, G. *J. Chem. Soc., Perkin Trans. 2* **1993**, 799.

(23) McRae, E. G. *J. Phys. Chem.* **1957**, *61*, 562.

(24) Reichardt, C.; Asharin-Fard, S.; Schäfer, G. *Liebigs Ann. Chem.* **1993**, 23.

(25) Beard, M. C.; Turner, G. M.; Schuttenmaer, C. A. *J. Am. Chem. Soc.* **2000**, *122*, 11541.

(26) Levinger, N. E.; Johnson, A. E.; Walker, G. C.; Barbara, P. F. *Chem. Phys. Lett.* **1992**, *196*, 159.

(27) Walker, G. C.; Åkesson, E.; Johnson, A. E.; Levinger, N. E.; Barbara, P. F. *J. Phys. Chem.* **1992**, *96*, 3728.

(28) Murov, S. L.; Carmichael, I.; Hug, G. L. *Handbook of Photochemistry*, 2nd ed.; Marcel Dekker: New York, 1993.